Title: Cyclic, condition-independent activity in primary motor cortex predicts corrective movement behavior

Author: Adam G. Rouse*

Affiliations:

Department of Neuroscience, University of Rochester, Rochester, NY, 14642, USA

Del Monte Institute for Neuroscience, University of Rochester, Rochester, NY

Corresponding Author and Lead Contact: *Please address correspondence to:

Adam G. Rouse
Department of Neuroscience
University of Rochester Medical Center
601 Elmwood Avenue, Box 603
Rochester, NY 14642
E-mail: adam_rouse@urmc.rochester.edu

Pages: 21
Figures: 4
Tables: 0
Movies: 0
Characters: characters

Conflict of Interest: The authors declare no competing financial interests.

Character count, including spaces (not including STAR methods): 32,614

Highlights

- Motor cortex activity displays cyclic dynamics for corrective movements
- Cyclic trajectories are similar for initial and subsequent corrective movements
- In both, cycle phase predicts the timing of peak speed and target contact
- Motor cortex encodes discrete sub-movements rather than continuous updating

eTOC Blurb

Rouse finds that the cyclic activity of primary motor cortex neuron populations is similar for initial reaches and subsequent corrective movements. Cycle phase predicts when movement speed peaks occur and when the cursor contacts the target.

Summary

Cyclic neural activity independent of target condition occurred during both initial reaching movements and multiple corrective movements as subjects performed a precision center-out task. The cyclic neural trajectories were similar during initial and corrective movements. For both, instantaneous cycle phase predicted when contact with the target occurred, even when the subject made multiple corrective movements. Moreover, the phase of the cyclic neural activity correlated with instantaneous movement speed. Neural activity during these corrective movements thus reveals encoding of discrete sub-movements rather than smooth and continuous updating of movement towards a target.

Keywords

Primary motor cortex, Population dynamics, Reaching, Aiming, Dimensionality reduction, Neural population, Corrective movements, Cyclic, State space, Dynamic Systems

Introduction

Corrective movements with sensorimotor feedback are critical for elegant motor control. While a single, discrete movement like a pointing gesture may be mostly ballistic, more precise aiming movements typically require an error correction phase (Woodworth, 1899; Craik, 1947; Abrams et al., 1990; Sainburg et al., 1999; Elliott et al., 2010). Yet the way motor areas of the brain are updated to encode and generate corrective movements remains relatively unexplored. For overlearned, mostly ballistic movements, a population of recorded neurons' firing rates have been observed to form a one-way, cyclic trajectory in the neural space (Yu et al., 2007). This has been argued to occur for even discrete movements like point-to-point reaching, in addition to inherently cyclic movements like locomotion (Grillner, 1985). If these dynamics are intrinsic to the neural architecture, this cyclic activity

might influence tasks when there is no clear benefit or even be suboptimal. For instance, without cyclic dynamics precise movements might be best accomplished with continuously updating corrections based on the current motor error. If such cyclic dynamics do exist, however, one would hypothesize that the timing of corrective movements would align with this cyclic neural activity.

Neural activity in primary motor cortex is not only related to various movement features but also has a large condition-independent component (Kaufman et al., 2016). Condition-independent neural activity is the change in a neuron's firing rate from baseline that happens regardless of the instructed movement for a particular trial within a given task. Techniques like demixed principal component analysis partition a neural population's activity into condition-independent modulation and the more classical neural tuning to task features (Kobak et al., 2016). This condition-independent activity is not a simple increase and decrease in firing rate for each neuron but has an inherent cyclical structure hypothesized to be related to intrinsic cortical dynamics (Churchland et al., 2012; Hall et al., 2014). The neural dimensions with the greatest cyclic activity can be identified and visualized with techniques such as jPCA. During movements, neural activity forms circular trajectories in these identified dimensions.

Almost all recent work examining this dynamic, cyclic neural structure has focused on overlearned, mostly ballistic movements with the subject making very few errors. Hall et al. (2014) did examine corrective submovements in an isometric wrist flexion/extension task and showed the behavior was correlated to cyclic local field potentials in motor cortex. Recent studies have also examined online correction with mechanical perturbations (Pruszynski et al., 2011) or jumps in targets (Stavisky et al., 2016) but these movements were experimentally perturbed and analyzed condition-dependent neural activity. Little work has focused on recorded spiking units in primary motor cortex during precision tasks with the subject freely correcting as needed.

Here, condition-independent neural activity during corrective movements was studied to test whether cyclic neural activity is behaviorally linked to subject initiated corrective movements. A precision center-out task that elicited visuomotor corrections to settle on a small target was used. The condition-independent modulation in the neural state space was calculated and a dynamical systems approach identified cyclic activity. A new analysis variable—condition-independent phase (CIφ)—is introduced to calculate the instantaneous phase of cyclic, condition-independent spiking activity and tested for its relationship to behavioral events.

Results

The precision center-out task was performed by two monkeys using a joystick to move a cursor to one of eight targets from a center starting position. The targets were located equidistant from and evenly distributed around the center with a small radial dimension. Because of the targets' small size, the cursor often exited the target before completing a required final hold with the monkey free to make supplemental, corrective movements to re-enter the target (see Supplemental Figure S1). The firing rates of simultaneously recorded single- and multi-unit activity in primary motor cortex during a precision center-out task were analyzed. Neural data were analyzed for both i) the initial movement periods from when the instructed target appeared until the target was contacted for the first time, and ii) any supplemental movement periods from when the cursor left the correct target until subsequent re-entry. Data were analyzed from 5 recording sessions from monkey P and 6 sessions from monkey Q. The dataset contained 1530 successfully completed trials with 49% of trials requiring at least one

supplemental movement after a leave target event for monkey P and 1503 trials with 32% of trials requiring supplemental movements for monkey Q. The distribution of the number of supplemental movements per trial and movement times are given in Supplemental Figure S2. Since the cursor was sometimes on the target boundary with very short excursions outside the target that likely did not require a volitional corrective movement, only supplemental movements that lasted at least 200 ms were included in subsequent analysis.

The analysis presented here identifies cyclic, condition-independent activity in the neural space and tests whether its timing is correlated with behavior. Condition-independent activity was defined as the average firing rates for individual units across all trials regardless of the movement condition (i.e. target location). The condition-independent activity was submitted to jPCA to identify the two-dimensional neural plane with the most rotational/cyclic activity. Since trials were of varying durations and many included supplemental movements, simple time alignment of trials was difficult. Instead a novel iterative algorithm was used to align and average the data based on the phase of cyclic neural activity and then the jPC neural plane that best fit this new alignment was re-calculated. This algorithm is described more fully in the methods. Once identified, individual trials' firing rates could then be projected and examined in this jPC neural plane.

As an example, the cursor and neural trajectory for a single trial is shown in Figure 1. The cursor trajectory (Figure 1A) shows that after the initial movement into the peripheral target boundaries there were two supplemental movement periods when the cursor passed through the target before correcting and re-entering the target again. When examining the cursor speed in Figure 1D, there were four peaks (indicated with arrows) when movement was fastest. These four peaks correspond to 1) the initial movement (between the yellow circle to yellow square) from the center to the target that then goes too far and passes the target, 2) a submovement in the first supplemental period (blue circle to blue square) to contact the target again but once more passes through the target, and 3 & 4) a pair of submovements in the second supplemental period (orange circle to orange square) with the first submovement occuring outside the target before the second returns to contact the target and successfully complete the trial. Interestingly, each of these speed peaks corresponds to the downward sloping phase of jPC_1. Likewise, the phase of jPC_1—which we define as the condition-independent phase (CIφ)—is between 0 and π for each of these speed peaks. Similarly, the three target contacts (square markers) always occurred when the CIφ was between 0 and π during these speed peaks. Thus, submovements within this trial were phase aligned with the cyclic, condition-independent brain activity.

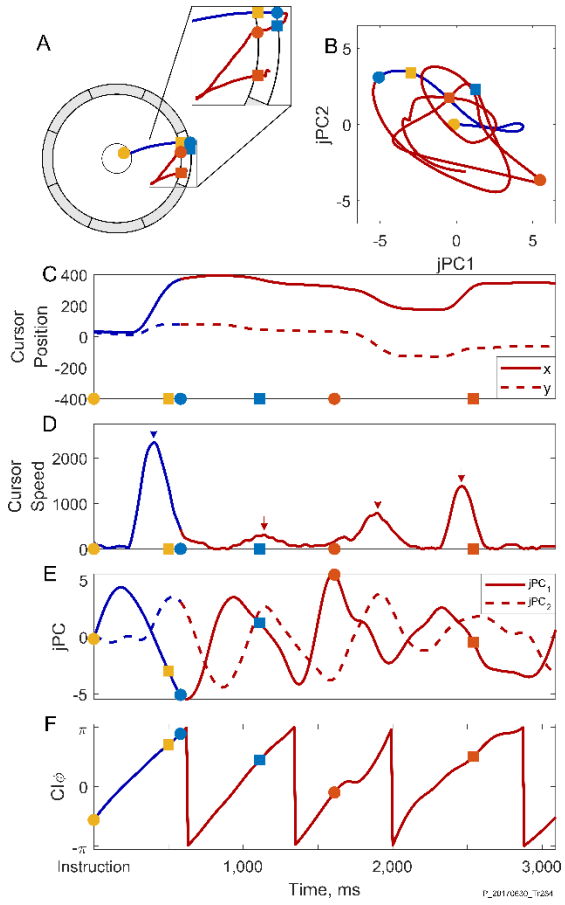

Figure 1. Example trial of the precision center-out task with corrective movements. A) The cursor position for a single trial reaching to the right target. Following the instruction (yellow circle), the cursor moves to and enters the target (yellow square). However, the cursor exits (blue and orange circles) and enters (blue and orange squares) the target two times before successfully completing the center hold. B) Neural activity in the jPC_1 and jPC_2 plane shows a cyclic trajectory with each contact (squares) occurring in a similar part of the trajectory following either instruction or leave target events (circles). C) The cursor position plotted as a function of time (horizontal dimension-solid line, vertical dimension-dashed line). D) The cursor speed showing occurrences of speed peaks. E) The jPC_1 (solid) and jPC_2 (dashed) neural dimensions plotted as a function of time. F) The condition-independent phase (CIφ)—calculated using the Hilbert transform of jPC_1 to estimate the instantaneous phase—showing four cycles that approximately align with the four cursor speed peaks.

The average neural trajectory was examined for both the initial movements as well as supplemental movements. The neural activity was projected into the neural plane with the most cyclic, condition-independent activity identified when jPCA was applied to all movement data. The average neural trajectories for both initial and supplemental movements are shown as projections in the jPC plane in Figure 2. The average trajectories of both the initial and supplemental movements follow a similar path for both animals. The trajectories start at the circle when either the target instruction (initial movements, blue) or cursor leave target (supplemental movements, red) events occurred. The trajectories then proceed in a counter-clockwise direction and are shown until 1000 ms after the initial instruction or 800 ms after leave target events. The orientation, direction, and speed of rotation of the neural trajectory are similar between initial and supplemental movements and was also similar between animals.

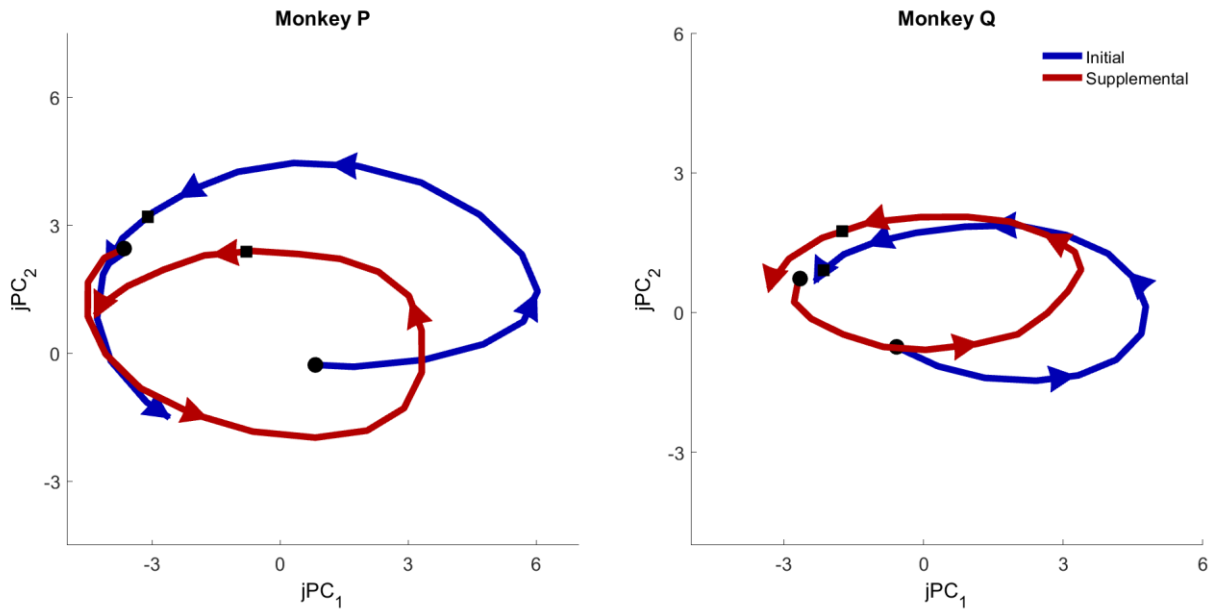

Figure 2. Similar condition-independent neural trajectories for initial and supplemental movements. Average neural trajectories of all initial and supplemental movements from a single recording session projected in the first jPC plane. Each datapoint is the average jPC_1 and jPC_2 values of all trials at a given phase (CIφ, see Methods). The starting point (black circle) for each trajectory is the mean CIφ at instruction for initial movements and at leave target for supplemental movements. Arrows indicate the average CIφ in 200 ms intervals from the start of each trajectory. The black square indicates the CIφ when 50% of initial movements had contacted or supplemental movements re-contacted the target.

To assess the consistency and alignment of cyclic, condition-independent neural activity with the behavioral task, the CIφ for all trials was aligned to the behavioral events of the task. The CIφ values were aligned to three behavioral events to display four different time periods: i) Instruction – the initial hold and initial movement period, ii) Leave target – supplemental movement periods (if one or more existed for a given trial), and iii) Final hold – the successful final hold period. The CIφ values were tested for a non-uniform, unimodal distribution across all four time periods—initial hold, initial movement, supplemental movement, and final hold—at all time points when data existed for >50% of trials. The CIφ values across all trials were non-uniformly distributed at all time points tested ($p<0.001$, Rayleigh test, Bonferroni corrected for multiple time points) suggesting the CIφ was consistently aligned with the task. The CIφ values are shown for 150 randomly selected trials across all recording sessions (Figure 3A). The CIφ is first aligned with Instruction. The CIφ values across trials have a similar slope before Instruction suggesting cyclic neural activity was present even during the initial hold period. At Instruction, the CIφ values continue with a similar slope but now have more similar time-aligned values with less variance than during the initial hold period. The most consistent CIφ values during initial movements across all trials were 260 ms and 420 ms after instruction with the smallest circular variance being 0.18 and 0.31 for monkey P and Q, respectively. The initial contacts are identified with squares and are separated by color for whether the CIφ progressed for 1, 2, or ≥3 cycles from Instruction (see Methods). For a majority of movements, a single upswing or cycle occurs until the cursor contacted the target (blue points). In some trials, however, two (orange) or more (yellow) CIφ cycles occur as the cursor did not contact the target

initially and required additional submovements (see also Figure 4). Next, the CIφ is aligned on all Leave target events when the cursor left the target and a corrective, supplemental movement was required. A similar consistent CIφ slope across trials is also observed for supplemental movements. Again a majority of supplemental movements are one CIφ cycle but two, three, or more cycles also exist. The final alignment point when the target was contacted for successful completion of a trial shows that the CIφ continued a similar upward slope.

The CIφ values aligned to target contacts were next examined. A majority of contacts with the target for both initial (Figure 3B) and supplemental (Figure 3D) movements occurred after CIφ=0 following an upward, consistently sloping CIφ indicating a cycle. These results suggest the cyclic, condition-independent neural activity—as measured with the CIφ—were consistently aligned with the behavioral timing of the task and progressed at a similar rate. The CIφ values at all target contacts were tested to determine if the cyclic, condition-independent neural activity was indeed predictive of this behavioral event. The distribution of all contacts was significantly non-uniform ($p<0.001$, Rayleigh test) for both animals with much more than half of all contacts—82% and 83% of contacts (monkey P and Q, respectively)—occurring within the half-cycle surrounding the circular mean of contact CIφ values (0.63π and 0.58π for monkey P and Q, respectively). The histogram of the CIφ for all target contacts separated by initial and corrective movements and by which CIφ cycle the contact occurred is shown in Figure 3C. There were significant cycle differences for both animals ($p<0.001$, Watson-Williams circular ANOVA test) with the largest effect being for the initial movements with only one CI cycle having a mean CIφ at contact of 0.73π and 0.69π (monkey P and Q, respectively). For the smaller submovements—either initial movements with two or more CI cycles and supplemental movements with at least one CI cycle—the differences were smaller with a mean CIφ always between 0.28π-0.52π. These results demonstrate CIφ was indeed predictive of when target contacts occurred.

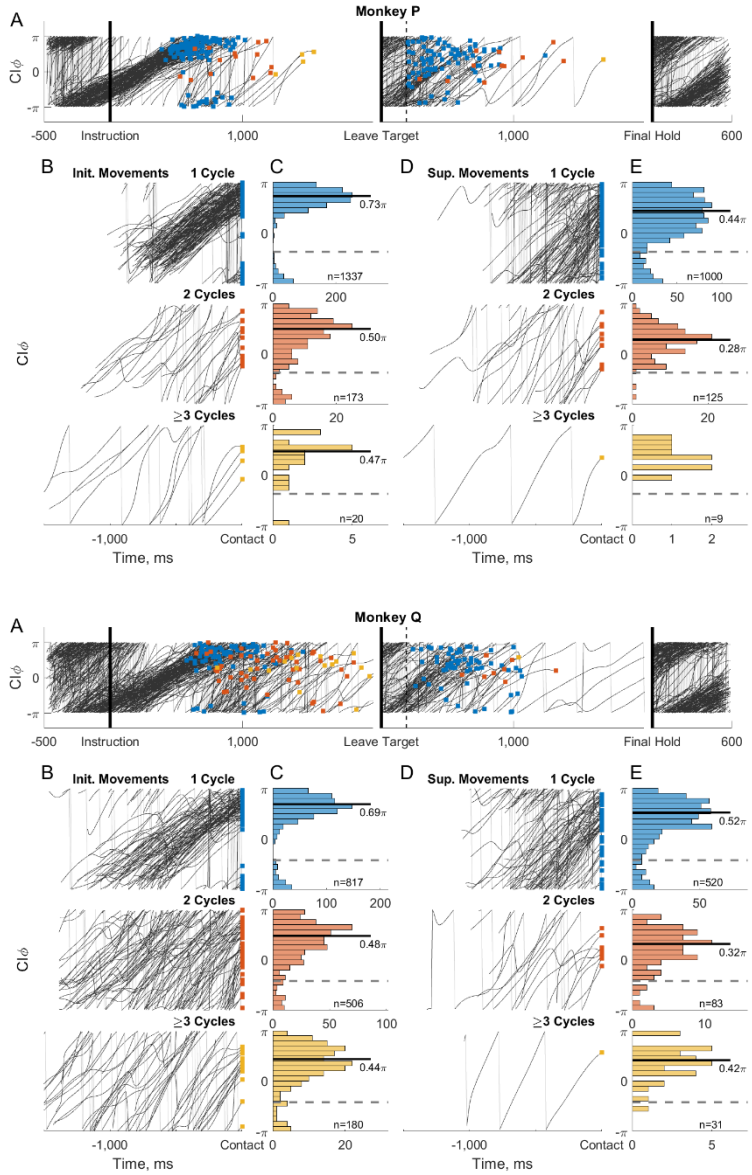

Figure 3. CIφ is correlated to behavioral events. A) The CIφ (wrapped between -π to +π) is plotted time aligned to: instruction including the preceding initial hold and subsequent initial movement (left), leave target (after previously entering the target) including the supplemental movements (center), and final contact with the target including the subsequent successful hold (right). 150 trials selected randomly across all recording sessions are shown for each animal. The target contacts—after both initial and supplemental movements—are shown with the color indicating whether there was 1 (blue), 2 (orange), and ≥3 (yellow) CIφ cycles. The dashed vertical line indicates 200 ms after the leave target event used as the minimum supplemental movement time included in this analysis. B & D) The CIφ is time aligned to contact with the target—after both initial (B) and supplemental (D) movements—and is separated by the number of CIφ cycles. C & E) Histogram of CIφ at target contact for initial movements (C) and supplemental movements (E). The solid lines indicate the mean CIφ for each cycle. The dashed lines indicate the cutoff used to define the cycle boundary and is one-half cycle from the global mean contact CIφ (across both initial and supplemental movements and all cycles).

Finally, the cursor speed as a function of CIφ was examined. The peaks and troughs of cursor speeds for most trials aligned with 2π cycles of CIφ (Figure 4A). The average speed as a function of CIφ for each monkey showed a clear periodicity (Figure 4B). The circular correlation between speed and CIφ was 0.45 and 0.41 ($p<0.001$) with the largest speeds occurring at CIφ = 0.47π and 0.39π (+2kπ) for monkeys P and Q, respectively (see Supplemental Figure S4). Finally, as the averaging and correlations could potentially be dominated by only large amplitude movements, the CIφ values when cursor peak speeds occurred were also calculated (see Methods). The peak speeds were indeed non-uniformly distributed ($p<0.001$, Rayleigh test) with a mean CIφ of 0.45π and 0.36π for monkeys P and Q, respectively (Figure 4C). These peaks were similarly distributed for both the initial and corrective parts of the movement with the peak speeds for the first cycle having slightly delayed CIφ values, similar to the delay in CIφ values when target contact occurred in the first cycle in Figure 3. Both the cyclic average speed and the non-uniform occurrence of peak speeds demonstrate that the movement speed was consistently correlated with cyclic, condition-independent brain activity.

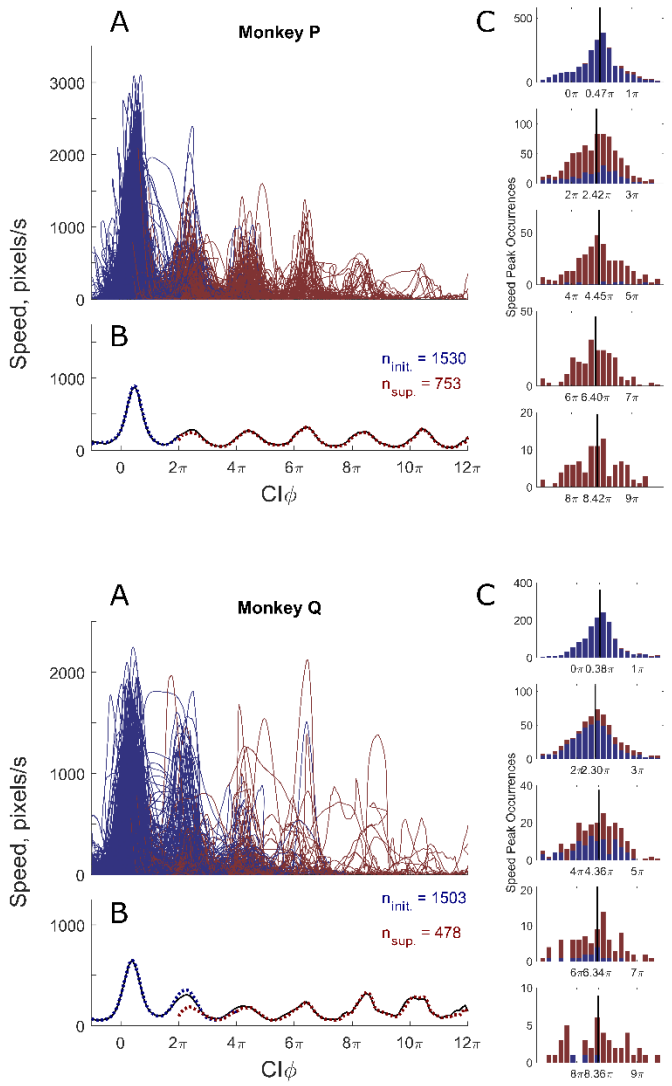

Figure 4. CIφ is correlated to movement speed. A) The movement speed—measured in pixels/s of instantaneous cursor movement—is plotted for 300 randomly selected trials as a function of condition-independent phase (CIφ). The initial movements from the center until first contacting the target are shown in blue. The red traces show the continuation of trials when the monkey left the target and required a supplemental movement to re-enter the target. The speed trajectories are cyclic with multiple peaks for initial movements that did not reach the target and required a second submovement (additional blue peaks) and supplemental movements after passing through the target (subsequent red peaks). B) The average speed plotted for all initial movements (blue, dotted line), supplemental movements (red, dotted line), and all movements combined (black line). C) Histogram of CIφ values at occurrences of cursor speed peaks. The histograms are separated by the number of CIφ cycles after the instruction. Speed peaks during both initial (blue) and supplemental (red) movements are shown.

Discussion

A consistent relationship between cyclic, condition-independent brain activity and the behavioral timing of corrective reaching movements was observed. The precision center-out task utilized small targets to elicit many trials that were not completed initially and required subsequent movements. The speed profiles of these subsequent movements and target contacts aligned with cyclic activity in primary motor cortex suggesting encoding of discrete submovements rather than smooth and continuous updating of movement towards the target. Discrete submovements have previously been described in behavioral studies of reaching (Pratt et al., 1994; Lee et al., 1997), turning a knob (Novak et al., 2000), isometric contractions (Massey et al., 1992; Hall et al., 2014), and object manipulation for tactile discrimination (Pruszynski et al., 2018). Modeling alternating periods of movements and updating have led to several descriptions consistent with predictive models of observed behavior such as Fitts's Law (Keele, 1968; Crossman and Goodeve, 1983; Meyer et al., 1988; Milner, 1992; Beamish et al., 2006). The experimental results and analysis techniques presented here provide new evidence of how neural activity is related to behaviorally observed submovements.

Similar cyclic neural activity in initial and corrective movements

Condition-independent neural activity has commonly been observed in motor tasks that are overtrained to be consistent across trials. Here, in a precision center-out task with considerable trial-to-trial variability, the condition-independent neural dynamics were observed to be similar for both initial as well as supplemental corrective movements and were cyclic. Examining the identified dimensions with the most cyclic activity showed similar neural activity for both initial and corrective movements. The magnitude of neural modulation in this space tended to be similar with the neural trajectory almost always having a similar orientation and direction.

Condition-independent phase aligned with behavioral events

The CIφ aligned with the task and progressed similarly for both initial and corrective movements. Notably, a majority of target contacts—during both the initial and supplemental movement periods—occurred within a limited range of CIφ values. The CIφ values were significantly non-uniformly distributed during instruction, initial movement, any corrective movements, and final hold. While the CIφ during initial movements were more consistent than supplemental movements, they both were significant and similarly aligned with a relatively constant slope. The CIφ thus represents a description of the cyclic neural activity that happens during any submovement and predicts when the subjects made movements to contact the target—either initially or when corrective movements were required.

Interestingly, the condition-independent neural activity also continued to rotate during holding states—instruction and final hold. The phase was non-uniform when aligned to Instruction and Final Contact with a consistent slope during these holding states. Although both holds had a random duration, it was of a limited range and the subjects could have still been anticipating upcoming movement. Additionally, since a bidirectional bandpass filter was used and the Hilbert transform integrates across time, the brain dynamics during movement may also have affected the calculated phases and alignment observed during holding periods. Further testing with greater variation of instruction and hold times and greater diversity of tasks will be needed to assess when cyclic, neural activity is perturbed by external events.

Condition-independent phase predictive of cursor speed

The cyclic CIφ values aligned with cursor speed. This further confirmed the observed cyclic neural dynamics were behaviorally relevant. The cursor speeds exhibited peaks and troughs that corresponded to a particular phase and suggests that the corrective movements were cyclic with separate submovements. Rather than continuously moving the hand toward the target at all times, the subjects' movements appeared as pulsatile bursts of joystick movement and presumably muscle contraction. While difficult to determine how much of the cyclic brain activity and behavior is intrinsic versus a cognitive strategy for this particular task, the observed results highlight the importance of cyclic neural dynamics in at least some corrective tasks. The cyclic dynamics of the condition-independent neural activity may also lead to better descriptions of the condition-dependent activity that encode task features, specifically the observation that direction encoding is often not fixed but shifts with different phases of movement (Churchland and Shenoy, 2007; Suminski et al., 2015; Suway et al., 2017).

The cyclic dynamics of corrective movements have important implications for brain-computer interfaces (BCI). To date, most BCI decoders are time-invariant both to the phase within a single movement and when multi-part movements or corrective movements occur. The decoders are typically built initially with observed or imagined movements that assume single, straight-line movements. When algorithms for updating BCI decoders consider the change in movement direction for corrective movements, it is assumed the intended path is updated continuously (Gilja et al., 2012; Shanechi et al., 2016). Experiments have suggested that BCI control can be improved with two states: active control and rest (Kim et al., 2011; Williams et al., 2013, 2016; Sachs et al., 2016). The ability to predict the phase of a movement—like CIφ presented here—might further allow for much better prediction of when the subject intends to move, contact the target, and make a corrective movement as well as enable encoders of movement direction that change with time. Finally, while some work has explored ways to input lost sensory information to replace lost function (Flesher et al., 2016; Mazurek and Schieber, 2017), how motor cortex naturally uses sensory feedback or would utilize artificial stimulation to encode subsequent corrective movements remains largely unexplored.

STAR Methods

Key Resources Table

Reagent or Resource	SOURCE	IDENTIFIER
Software and Algorithms		
Matlab	**Mathworks**	**https://www.mathworks.com/products/matlab.html**
Circular Statistics Toolbox	**Mathworks File Exchange, Philipp Berens**	**https://www.mathworks.com/matlabcentral/fileexchange/10676-circular-statistics-toolbox-directional-statistics**
Multichannel Acquisition Processor Software	**Plexon Inc. Plexon**	**http://plexon.com/products/map-software**
Offline Sorter	**Plexon Inc. Plexon**	**http://plexon.com/products/offline-sorter**
Other		
MAP Data Acquisition System Plexon	**Plexon Inc. Plexon**	**https://plexon.com/products/map-data-acquisition-system-plexon/**
Floating Microelectrode Arrays (FMAs)	**Microprobes for Life Sciences**	**https://www.microprobes.com/products/multichannel-arrays/fma**
Model 212 Joystick	**PQ controls**	**http://www.pqcontrols.com/m212.php**
24" LCD Display Model P2412H	**Dell Inc.**	**https://www.dell.com/ed/business/p/dell-p2412h/pd**

Non-human primates

Two male rhesus monkeys, P and Q (weight 11 and 10 kg, ages 7 and 6 years old, respectively), were subjects in the present study. All procedures for the care and use of these nonhuman primates followed the Guide for the Care and Use of Laboratory Animals and were approved by the University Committee on Animal Resources at the University of Rochester, Rochester, New York.

Task

The experimental task was performed by the monkey using a joystick to control a cursor on a 24" LCD display. The monkey manipulated a custom, 18 cm long, cylindrical rod attached to the joystick housing. The joystick moved freely with minimal resistance as the spring mechanism for providing centering, restorative force was removed. The cursor directly represented measured joystick position and was allowed to move within a 1000x1000 pixel workspace centered on the display. The cursor

workspace limits were slightly within the physical limits of the joystick. The cursor on the display was a small cross that represented a single point in the workspace.

The precision center-out task consisted of a set of eight targets located equidistance and equally spaced in 45˚ intervals around a center, home target (Figure 1 and Supplemental Figure S1). The center target had a radius of 75 pixels. Each center-out target—defined in polar coordinates—spanned an angle of 45˚ and a distance of 325-375 pixels from the center for a small 50-pixel radial thickness. During each experimental session, two other sets of 8 center out targets with a larger 200-pixel radial thickness were also included: i) larger targets also spanning 45˚, and ii) narrower targets only spanning 15˚. All 24 targets (3 sizes x 8 locations) were presented pseudorandomly in equal amounts throughout a session. Only the trials for the eight targets with the smaller, 50-pixel radial target thickness are presented in the current analysis and results.

For each trial, the subject acquired the home target and performed a required initial hold ranging from 300-500 ms. At the end of the initial hold, the instruction occurred with the desired target changing colors to green. Following instruction, the monkey was allowed to move immediately and allowed 2,000 ms to contact the correct target. The outline of all targets changed colors providing visual feedback when the cursor was within the target boundaries. After contacting the desired target, the cursor was required to remain within the target for a variable hold time of 500-600 ms. If the cursor left the target during a final hold, the monkey was allowed an additional 2,000 ms following each leave target event to contact the target again and complete a final hold. If the cursor remained outside the target for greater than 2 s, the trial was aborted and excluded from the present analysis. Once a successful final hold of 500-600 ms was completed, the animal received a liquid reward. Both the required initial and final hold times for each trial were randomly sampled from a uniform distribution. The custom software for task control sampled the joystick data, updated the scene, and stored the cursor position (equivalent to joystick position) data and trial event times—initial hold start, instruction, contact target(s), leave target(s) (if any occurred), and final hold end—at 100 Hz.

The initial movement time window was defined as the period from when the target instruction appeared until the correct target was first contacted. The supplemental movement window was defined as any time the cursor left the correct target until it re-entered the correct target. For analysis shown in Figures 2 and 3, only supplemental movements lasting longer than 200 ms were used as shorter movement times likely did not include a volitional corrective movement.

For finding the occurrences of cursor speed peaks in Figure 4C, the cursor speed for each trial was submitted to a peak finding algorithm that identified local maxima (*findpeaks* function in Matlab). Cursor speeds were identified as peaks provided they met the following criteria: i) it was a maximum value at least 200 ms away from any larger peaks, ii) the peak speed was greater than 200 pixels/s, and iii) the peak's prominence— the height difference between the peak and the larger of the two adjacent troughs (minimum speed before encountering a larger peak)—was at least 50% of the absolute height of the peak.

Data Collection

Floating microelectrode arrays (MicroProbes) were implanted in the anterior bank of the central sulcus to record from primary motor cortex (M1) in each monkey, using methods described in detail

previously (Mollazadeh et al., 2011; Rouse and Schieber, 2016). For monkey P, recordings were collected from six 16-channel arrays implanted in M1. For monkey Q, two 32-channel arrays and one 16-channel array in M1 were used. Channels with spiking activity were thresholded manually on-line and spike-snippets and spike times were collected with the Plexon MAP data acquisition system. The spike snippets were sorted off-line—first with the automatic valley seeking algorithm in Plexon Offline Sorting software and then with a custom, semi-automated algorithm (Rouse and Schieber, 2016). Both single- and multi-unit recordings were used in the present analysis.

Data Analysis

The firing rates for individual units were estimated by convolving spike times with a Gaussian filter (σ=50 ms). The firing rates were estimated with 10 ms bin resolution for 100 Hz signals to match the joystick data and events. The firing rates were then square-root transformed to equalize variance between high and low firing rates (Kihlberg et al., 1972; Snedecor and Cochran, 1980; Ashe and Georgopoulos, 1994).

This work introduces a new analysis variable—condition-independent phase (CIφ)—which estimates at each time the instantaneous phase of the neural dimension with the most cyclic, condition-independent activity. The novel algorithm to calculate CIφ is iterative and involves three steps described in detail below: i) Each unit's firing rate is averaged across all trials to determine its condition-independent firing rate. ii) Dimensionality reduction is performed using PCA and jPCA on the condition-independent firing rates to identify the neural plane with the most rotational/cyclic condition-independent activity. iii) The instantaneous phase is calculated using the Hilbert transform on the first jPC dimension for all data points. A schematic of the iterative algorithm is shown in Supplemental Figure S3.

i) Trial averaging to identify condition-independent activity

The condition-independent neural activity is the average firing rate for each recorded spiking unit for all experimental trials regardless of the movement condition (ie target location). For classic neurophysiology experiments, this can be calculated by averaging time-aligned data. However, it is more challenging to time-align data for a task with many corrective movements. Data was therefore aligned based on each time-point's calculated CIφ rather than absolute time.

Since CIφ depends on the averaged condition-independent activity, an iterative approach was used. An initial estimate using simple time-alignment averaging was used for the first iteration. Data for this initial guess was aligned to instruction for initial movements and leave target for supplemental movements. For each subsequent iteration, the condition-independent firing rates for each unit were calculated by averaging all data points when the CIφ values were similar. The average firing rate was estimated using a sliding window of CIφ values with a step size of $\pi/50$ and a window size of $\pi/25$ to generate 100 equally spaced samples ranging from $-\pi$ to π.

ii) PCA and jPCA to identify rotational/cyclic neural activity

Next, the condition-independent firing rates were submitted to PCA and jPCA to identify the neural dimensions with the most cyclic activity. PCA was performed on the high-dimensional neural space to reduce the condition-independent firing rates to the six dimensions with the most variance. jPCA was then performed on this six dimensional space. jPCA is a dimensionality reduction technique to

identify the neural planes with the most rotational activity and is more fully described in Churchland et al (2012). Briefly, jPCA fits a first order dynamical system model to the neural activity to predict change in firing rate based on the current firing rate. The transform matrix of this model can be separated into a symmetric matrix representing pure scaling and a skew-symmetric matrix representing pure rotational dynamics. By taking the eigendecomposition of the skew-symmetric matrix, we obtain pairs of purely imaginary eigenvalues and corresponding eigenvectors that define planes of rotation in the neural space rank-ordered from greatest to least rotation. In the present analysis, only the first plane with the greatest rotation was used. Additionally, to obtain a consistent CIφ across recording sessions, jPC_1 was defined as the dimension in the jPC_1 and jPC_2 plane with the most variance. The positive jPC_1 direction was defined as having more positive than negative coefficients in the neural space which corresponds to the direction where more units have an increased firing rate. Choosing this convention causes an increase in jPC_1 to generally align with the onset of initial movement, since a majority of units increase firing rates at the onset of movement.

iii) Instantaneous phase estimate

Finally, the instantaneous phase of jPC_1 was estimated by i) bidirectional bandpass filtering of jPC_1 between 0.5-5 Hz with a 1st order Butterworth filter, ii) performing the Hilbert transform of the filtered signal (s_1) to generate a transformed signal ($\hat{s}_1$) that is a 90˚ phase shift of every Fourier component in the frequency domain to create an analytic representation of jPC_1, and iii) calculating the angle of the resulting analytic signal ($s_1 + i\hat{s}_1$) to estimate the instantaneous phase, which we call the condition-independent phase (*CIφ*).

$$\text{i)} \quad s_1(t) = filt_{0.5-5Hz}[jPC_1(t)]$$
$$\text{ii)} \quad \hat{s}_1(t) = \mathcal{H}[s_1(t)]$$
$$\text{iii)} \quad CI\phi\,(t) = \arg\{s_1(t) + i\hat{s}_1(t)\}$$

The bandpass filtering reduces the low-frequency drift and high-frequency variability in jPC_1 to generate a more consistent subsequent phase estimate. The condition-independent phase (CIφ) thus represents the instantaneous phase in the dimension of the neural space that has the most cyclic, condition-independent activity.

The neural activity in the jPC_1 and jPC_2 dimensions in Figure 2 were averaged by aligning trials based on their CIφ. This method was selected as it provided a more similar comparison between the initial and supplemental movements' rotational dynamics than time as the supplemental movements were not as precisely aligned in time to the leave target events as the initial movements to instruction. The average firing rates in the jPC_1 and jPC_2 dimensions were estimated using a sliding window of CIφ values with a step size of π/50 and a window size of π/25 starting with the average CIφ at instruction and leave target and ending with the average CIφ 1000 ms later for initial movements and 800 ms later for supplemental movements.

The cycles of CIφ in Figure 3 were counted by using the unwrapped (*unwrap* function in Matlab), continuous CIφ starting at either instruction or leave target. The starting CIφ values at instruction or

leave target were defined to be within +/-π radians of the mean CIφ starting value across all trials. The mean starting CIφ values were calculated separately for instruction and leave target and separately for each monkey and defined to be between -2π and 0. The center of cycles were defined by the circular mean contact CIφ for each monkey and incremented by $2k\pi$ with the boundaries for each cycle being +/-π radians around these centers. In Figure 4 the unwrapped CIφ is calculated with respect to the starting CIφ values at instruction which is again wrapped to be within +/-π radians of the mean CIφ starting value for each animal.

All circular statistics—mean, variance, correlation, Rayleigh test for non-uniformity, and Watson-Williams test (circular one-way ANOVA)—were calculated with CircStat, a Circular Statistics Toolbox for Matlab (Berens, 2009).

Acknowledgements

The author thanks Dr. Marc H. Schieber for many helpful discussions and editorial comments. The author thanks Dr. Gil Rivlis for technical advice and comments. This work was supported by National Institute of Neurological Disorders and Stroke grant K99NS101127 to A.G.R.

Author Contributions

Conceptualization, Methodology, Investigation, Writing, and Funding Acquisition performed by A.G.R.

Declaration of Interests

The author declares no competing interests.

References

Abrams, R.A., Meyer, D.E., and Kornblum, S. (1990). Eye-hand coordination: oculomotor control in rapid aimed limb movements. J. Exp. Psychol. Hum. Percept. Perform. *16*, 248–267.

Ashe, J., and Georgopoulos, A.P. (1994). Movement parameters and neural activity in motor cortex and area 5. Cereb Cortex *6*, 590–600.

Beamish, D., Bhatti, S.A., MacKenzie, I.S., and Wu, J. (2006). Fifty years later: A neurodynamic explanation of Fitts' law. J. R. Soc. Interface *3*, 649–654.

Berens, P. (2009). CircStat : A MATLAB Toolbox for Circular Statistics. J. Stat. Softw. *31*, 1–21.

Churchland, M.M., and Shenoy, K. V (2007). Temporal complexity and heterogeneity of single-neuron activity in premotor and motor cortex. J. Neurophysiol. *97*, 4235–4257.

Churchland, M.M., Cunningham, J.P., Kaufman, M.T., Foster, J.D., Nuyujukian, P., Ryu, S., and Shenoy, K. V (2012). Neural population dynamics during reaching. Nature *487*, 51–56.

Craik, K.J.W. (1947). Theory of the human operator in control systems. I. the operator as an engineering system. Br. J. Psychol. *38*, 56–61.

Crossman, E.R., and Goodeve, P.J. (1983). Feedback control of hand-movement and Fitts' Law. Q. J. Exp. Psychol. *35*, 251–278.

Elliott, D., Hansen, S., Grierson, L.E., Lyons, J., Bennett, S.J., and Hayes, S.J. (2010). Goal-Directed Aiming: Two Components but Multiple Processes. Psychol. Bull. *136*, 1023.

Flesher, S.N., Collinger, J.L., Foldes, S.T., Weiss, J.M., Downey, J.E., Tyler-Kabara, E.C., Bensmaia, S.J., Schwartz, A.B., Boninger, M.L., and Gaunt, R.A. (2016). Intracortical microstimulation of human somatosensory cortex. Sci. Transl. Med. *8*, aaf8083.

Gilja, V., Nuyujukian, P., Chestek, C.A., Cunningham, J.P., Yu, B.M., Fan, J.M., Ryu, S., and Shenoy, K. V (2012). A brain machine interface control algorithm designed from a feedback control perspective. Conf. Proc. IEEE Eng. Med. Biol. Soc. *2012*, 1318–1322.

Grillner, S. (1985). Neurobiological bases of rhythmic motor acts in vertebrates. Science *228*, 143–149.

Hall, T.M., de Carvalho, F., and Jackson, A. (2014). A common structure underlies low-frequency cortical dynamics in movement, sleep, and sedation. Neuron *83*, 1185–1199.

Kaufman, M.T., Seely, J.S., Sussillo, D., Ryu, S.I., Shenoy, K. V, and Churchland, M.M. (2016). The largest response component in motor cortex reflects movement timing but not movement type. ENeuro *3*, ENEURO.0085-16.2016.

Keele, S.W. (1968). Movement control in skilled motor performance. Psychol. Bull. *70*, 387–403.

Kihlberg, J.K., Herson, J.H., and Schotz, W.E. (1972). Square Root Transformation Revisited. J. R. Stat. Soc. *21*, 76–81.

Kim, S.-P., Simeral, J.D., Hochberg, L.R., Donoghue, J.P., Friehs, G.M., and Black, M.J. (2011). Point-and-click cursor control with an intracortical neural interface system by humans with tetraplegia. IEEE Trans. Neural Syst. Rehabil. Eng. *19*, 193–203.

Kobak, D., Brendel, W., Constantinidis, C., Feierstein, C.E., Kepecs, A., Mainen, Z.F., Qi, X.L., Romo, R., Uchida, N., and Machens, C.K. (2016). Demixed principal component analysis of neural population data. Elife *5*, 1–36.

Lee, D., Port, N.L., and Georgopoulos, A.P. (1997). Manual interception of moving targets. Exp. Brain Res. *116*, 421–433.

Massey, J.T., Lurito, J.T., Pellizzer, G., and Georgopoulos, a P. (1992). Three-dimensional drawings in isometric conditions: relation between geometry and kinematics. Exp. Brain Res. *88*, 685–690.

Mazurek, K.A., and Schieber, M.H. (2017). Injecting Instructions into Premotor Cortex. Neuron *96*, 1282–1289.e4.

Meyer, D.E., Abrams, R.A., Kornblum, S., Wright, C.E., and Smith, J.E.K. (1988). Optimality in human motor performance: Ideal control of rapid aiming movements. Psychol. Rev. *95*, 340–370.

Milner, T.E. (1992). A model for the generation of movements requiring endpoint precision. Neuroscience *49*, 487–496.

Mollazadeh, M., Aggarwal, V., Davidson, A.G., Law, A.J., Thakor, N. V, and Schieber, M.H. (2011). Spatiotemporal variation of multiple neurophysiological signals in the primary motor cortex during dexterous reach-to-grasp movements. J. Neurosci. *31*, 15531–15543.

Novak, K.E., Miller, L.E., and Houk, J.C. (2000). Kinematic properties of rapid hand movements in a knob turning task. Exp. Brain Res. *132*, 419–433.

Pratt, J., Chasteen, A.L., and Abrams, R.A. (1994). Rapid aimed limb movements: age differences and practice effects in component submovements. Psychol. Aging *9*, 325–334.

Pruszynski, J.A., Kurtzer, I., Nashed, J.Y., Omrani, M., Brouwer, B., and Scott, S.H. (2011). Primary motor cortex underlies multi-joint integration for fast feedback control. Nature *478*, 387–390.

Pruszynski, J.A., Flanagan, J.R., and Johansson, R.S. (2018). Fast and accurate edge orientation processing during object manipulation. Elife *7*, e31200.

Rouse, A.G., and Schieber, M.H. (2016). Spatiotemporal Distribution of Location and Object Effects in Primary Motor Cortex Neurons during Reach-to-Grasp. J. Neurosci. *36*, 10640–10653.

Sachs, N.A., Ruiz-Torres, R., Perreault, E.J., and Miller, L.E. (2016). Brain-state classification and a dual-state decoder dramatically improve the control of cursor movement through a brain-machine interface. J Neural Eng *13*, 016009.

Sainburg, R.L., Ghez, C., and Kalakanis, D. (1999). Intersegmental dynamics are controlled by sequential anticipatory, error correction, and postural mechanisms. J. Neurophysiol. *81*, 1045–1056.

Shanechi, M.M., Orsborn, A.L., and Carmena, J.M. (2016). Robust Brain-Machine Interface Design Using Optimal Feedback Control Modeling and Adaptive Point Process Filtering. PLoS Comput. Biol. *12*, 1–29.

Snedecor, G., and Cochran, W. (1980). Statistical Methods (Ames, IA: Iowa State UP).

Stavisky, S.D., Kao, J.C., Ryu, S.I., and Shenoy, K. V (2016). Motor Cortical Visuomotor Feedback Activity Is Initially Isolated from Downstream Targets in Output-Null Neural State Space Dimensions. Neuron *95*, 195–208.e9.

Suminski, A.J., Mardoum, P., Lillicrap, T.P., and Hatsopoulos, N.G. (2015). Temporal evolution of both premotor and motor cortical tuning properties reflect changes in limb biomechanics. J. Neurophysiol. *113*, 2812–2823.

Suway, S.B., Orellana, J., McMorland, A.J.C., Fraser, G.W., Liu, Z., Velliste, M., Chase, S.M., Kass, R.E., and Schwartz, A.B. (2017). Temporally Segmented Directionality in the Motor Cortex. Cereb. Cortex *12*, 1–14.

Williams, J.J., Rouse, A.G., Thongpang, S., Williams, J.C., and Moran, D.W. (2013). Differentiating closed-loop cortical intention from rest: building an asynchronous electrocorticographic BCI. J. Neural Eng. *10*, 046001.

Williams, J.J., Tien, R.N., Inoue, Y., and Schwartz, A.B. (2016). Idle state classification using spiking activity and local field potentials in a brain computer interface. 2016 38th Annu. Int. Conf. IEEE Eng. Med. Biol. Soc. 1572–1575.

Woodworth, R.S. (1899). The accuracy of voluntary movement. Psychol. Rev. *3*, 1–119.

Yu, B.M., Kemere, C., Santhanam, G., Afshar, A., Ryu, S., Meng, T.H., Sahani, M., and Shenoy, K. V (2007). Mixture of trajectory models for neural decoding of goal-directed movements. J. Neurophysiol. *97*, 3763–3780.

SUPPLEMENTAL INFORMATION

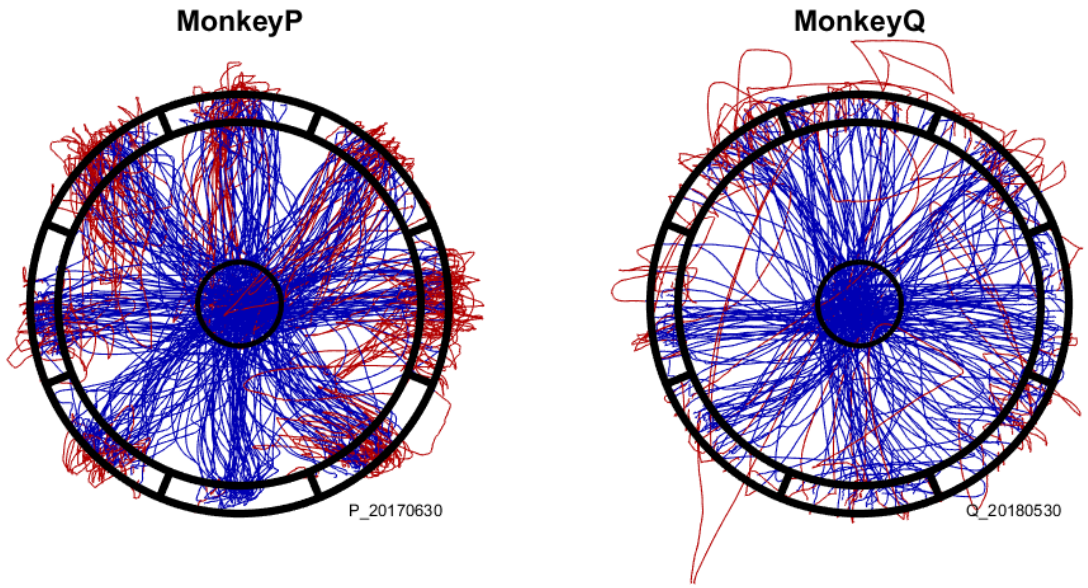

Supplemental Figure S1. Initial and supplemental cursor trajectories. Related to Figure 1. The cursor trajectories for all successful movements to all 8 shallow targets is shown for one recording session with each monkey. All trials start at the center circle with initial movements to the instructed target shown in blue. The supplemental movements are shown in red for all trials where the cursor left the target and the subject then corrected and re-entered the target to successfully complete the trial.

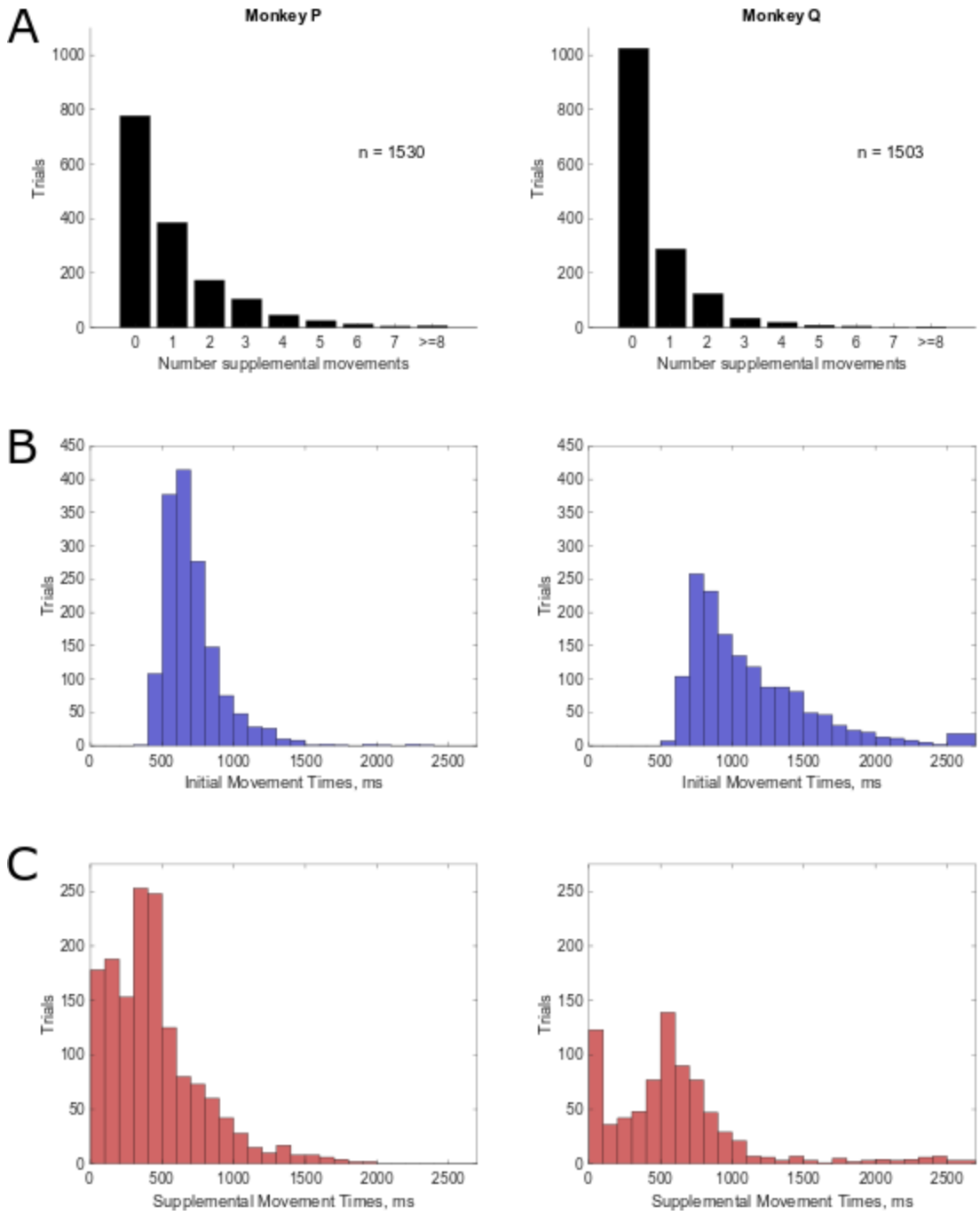

Supplemental Figure S2. Supplemental movement counts and movement times. Related to Figure 1. A) The number of supplemental movements in all successful trials for each monkey. B) Initial movement times from target instruction until initial contact with the target. Monkey Q had more long movement times resulting from making more initial movements that stopped before the target and required a corrective submovement. C) Supplemental movement times from leaving the target until re-contacting the target. The supplemental movement times were bimodally distributed with short duration times likely representing not volitional corrective movements but rather instances when the cursor was near the target boundary and drifted briefly outside.

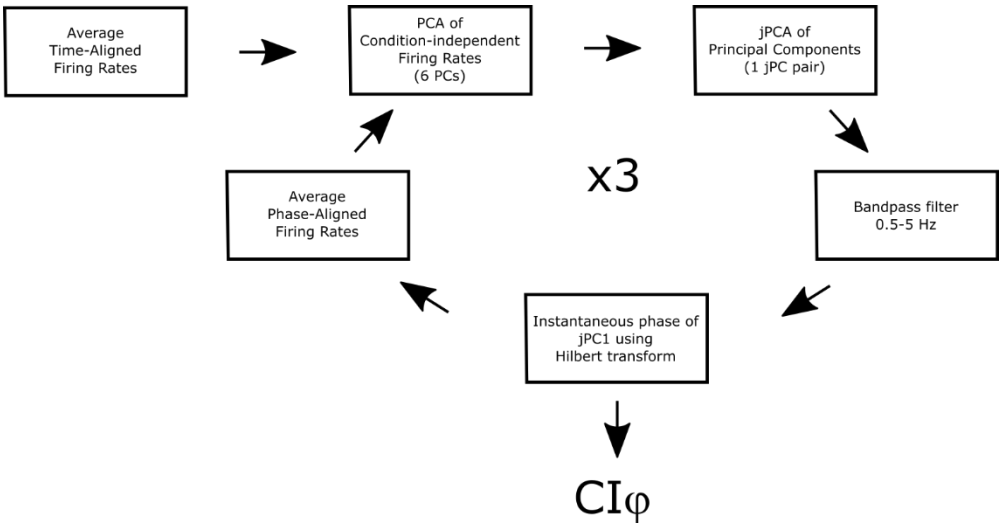

Supplemental Figure S3. Schematic of CIϕ estimation. Related to Figure 2. The cyclic condition-independent neural activity was estimated using an iterative technique. After initial time-alignment and averaging of the firing rates, PCA and jPCA was performed to estimate the dimensions neural activity with the greatest cyclic condition-activity were identified. Using the phase of this first jPC dimension, the firing rates were realigned for averaging. The PCA and jPCA were again performed a total of three times. The final CIϕ was then used for the presented analysis.

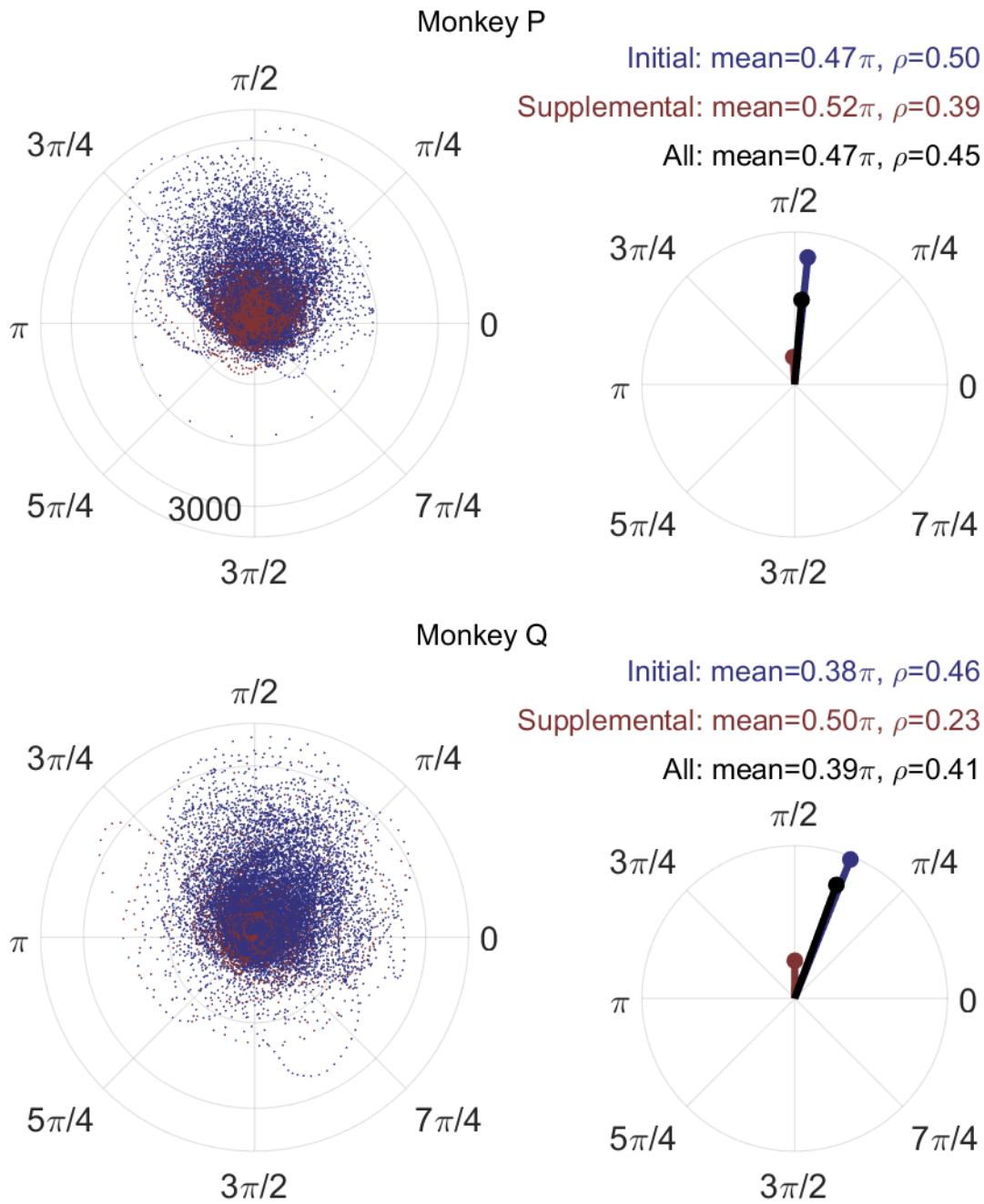

Supplemental Figure S4. Cursor speed relative to CIϕ. Related to Figure 4. Instantaneous cursor speed is shown in the polar plot as a function of CIϕ (left panel). The circular mean was calculated for all initial movement data points, all supplemental movement data points, all data points combined (right panel). A significant correlation between between CIϕ and cursor speed with a consistent mean phase between 0.38π-0.52π was observed for both monkeys and both trial periods.